Chapter 71
Dracar: An Estuarine Transfer Function to Predict Dissolved Pollutant Fluxes to the Sea. Application for Radionuclides

Adrien Delaval, Céline Duffa, Ivane Pairaud, and Olivier Radakovitch

Abstract Estuaries at the river-sea interface are capable of modulating the export of water and pollutants to the sea through their circulation and reactivity leading to large uncertainties. As a result, coupling large scale models of pollutant transfer in aquatic ecosystems (river and sea) requires an interfacing, even minimal, between them. We propose to reduce these uncertainties with an estuarine transfer function, DRACAR (Désorption des RAdionuCléides à l' interfAce littoRale) developed in Rstudio. This interface consists of a preliminary description of estuary's stratification using simplified "coupled shallow water equations". Then, consistency in the exchange of water, dissolved elements and potential energy is ensured by a box model (Sun et al. in Ocean Model 112:139–153, 2017 [1]). Main hydrodynamic processes such as entrainment, diffusion and boundary layer turbulence are reproduced with little need for calibration and the model is particularly suitable for stratified estuaries. Finally, a residence time in the inner plume is calculated by the "fresh water fraction method" to take into account the possible reaction kinetics such as radionuclides decay or speciation with suspended sediments. This interface provides a more reliable source term to the sea for modelling the transfer of dissolved radionuclides in a river-sea continuum in case of events of accidental release.

Keywords Box-model · Coupled modelling · River-sea continuum · Salt-wedge

71.1 Introduction

Rivers bring water, particles and pollutants to the sea. The estuary, at the interface, is a key element in the transfer of the latter. Many pollutants, including trace metals, come mainly from anthropogenic sources located on the watershed. For example,

A. Delaval (✉) · C. Duffa · O. Radakovitch
IRSN (Institut de Radioprotection et de Sûreté Nucléaire), PSE-ENV/SRTE/LRTA, 13115 Saint-Paul-Les-Durance, France
e-mail: adrien.delaval@irsn.fr

I. Pairaud
UMR 6523 CNRS, IFREMER, IRD, UBO, Laboratoire D'Océanographie Physique et Spatiale, 29280 Plouzané, France

P. Gourbesville and G. Caignaert (eds.), *Advances in Hydroinformatics*, Springer Water,
https://doi.org/10.1007/978-981-19-1600-7_71

anthropogenic radionuclides originate from atmospheric deposition on the watershed or from direct discharge into the by the nuclear industry [2].

Estuarine processes control water circulation, suspended matter dynamics and trace metal fuxes. This is also true for most of the mediterranean estuaries which are highly stratified or "salt-wedge" type. Between the fresh or brackish water flowing seaward and the underlying seawater, there is a velocity shear. It induces entrainment of seawater into the upper brackish layer and movement of seawater towards the land just below the upper layer. As a result of entrainment and turbulent diffusion the upper layer (inner plume) becomes progressively saltier from the head of the estuary towards its mouth. In addition, a landward flow is formed deeper in the marine layer to compensate for the loss of water to the upper layer and the movement of seawater towards the sea just below the upper layer [3]. In terms of contaminant dynamics, the surface plume and the marine layer have opposite functions. The marine layer advects salt water over tens of kilometers, but also potential pollutants, and brings them to the surface plume. The plume quickly exports river inputs to the sea, the low salinity may be sufficient to trigger metals desorption or complexation reactions [4]. These processes modulate pollutant dissolved input, the most bioavailable fraction, into the marine environment. Modeling the transfer of these pollutants over the entire continuum is a necessary approach with a view to forecaste and mitigate pollution at a time when these pressures are increasing across the continuum.

The Institute of Radioprotection and Nuclear Safety (IRSN) is working on radionuclides riverine inputs to the sea. Key radionuclides for radioprotection such as ^{137}Cs or ^{60}Co are subject to desorption processes. Unpublished laboratory results show that their dissolved activities is up to 5 times higher in seawater than in freshwater. As a result, estuarine processes must be taken into account.

The operational approach chosen to ensure the continuum is the combination of a river hydrodynamic model and a marine hydrodynamic model [5]. When it comes to stratified estuaries, classical 1D stream flow models are not able to reproduce stratification while 3D marine hydrodynamic models often use too large mesh sizes to reproduce the dynamics of stratified estuaries, which are generally shallow and of small width. In addition, the flow and hydrology in rivers are not accurately reproduced in ocean models. The river discharge is imposed with zero salinity and arbitrarily distributed either horizontally or vertically over several grid cells. Those approaches neglect some estuarine physical processes that modify river inputs before they reach the open ocean [1]. Solutions exist, such as refining the meshes, embeding estuary nested configuration at higher horizontal resolution, or using a third externalized model. However, these solutions can be costly in terms of calculation and calibration time and could be unnecessary when we seek to assess the transfer capacities of the estuary to the marine system as a main approach rather than to describe water quality status at a precise location in the estuary.

As a first approach, few parameters are required to address the circulation and trace metal reactivity of an estuary: the flow out of the plume, the inflow of the salt intrusion, the average salinity of the estuary (governing speciation reactions) and the flushing time of water and particles in the estuary [6, 7]. Box models are able to provide estimates of these parameters. The precision of these box-models is

increased if their dimensions and exchange surface evolve with hydrodynamic conditions (flow/tide). In this context, this study presents the development of an interface, DRACAR, adapted to stratified estuaries which calculates the exchanges and the reactivity at the river-sea interface. This interface consists of a preliminary dimensioning of the box-model dimensions (length and stratification) according to hydrodynamic conditions. The exchanges in the box-model are then expressed in the form of balance equations. Solving these equations provides the parameters governing the transfer of dissolved reactive pollutants from the river to the sea.

An application is given for the export of ^{137}Cs from the Rhone River and its salt-wedge estuary. This is a strategic river in terms of radioprotection since the Rhone valley has 4 nuclear power plants in process and a spent fuel reprocessing center, under dismantlement since 1997 [2].

71.2 Material and Methods

71.2.1 Field Study and Data

The Rhone River basin has an area of approximately 97,800 km^2 and drains several areas including the Alps, the Jura, and the Cevennes. The mean annual flow discharge at the downstream is approximately 1500 $m^3\ s^{-1}$, based on [8]. The Rhone is characterized by large inter-annual flow and sediment flux variability due to highly variable rainfall patterns and lithology within the catchment [9]. This natural variability is enhanced by a series of hydroelectric dams [10]. According to Ibañez et al. [11], under the mean annual flow discharge salt-water is able to intrude into the Rhone River bed over tens of kilometers depending on the discharge. The longest intrusion is 36 km, salt-water progression being stopped by a natural threshold (Seuil de Terrin) at pK 294.

The Rhone River hourly discharges have been provided by the C.N.R (Compagnie Nationale du Rhône) thanks to the Rhone Sediment Observatory (OSR program). They were measured at the SORA station, in the city of Arles located 47 km upstream of the Rhone River mouth (Fig. 71.1). It must be noted that the Rhone River splits in two branches upstream of this station (PK 280): the Grand Rhone and the Petit Rhone. The station reports the discharge for the Grand Rhone River only, which represents about 90% of the total Rhone River discharge [8]. In our case we focus only on the Grand Rhone outlet. Limnimetric data were available in Grand-Boisviel provided by the CNR. Additionnal limnimetric data as well as surface salinity data were available at Barcarin located 15 km upstream of the mouth [12]. Liminimetric and salinity used were registered between 2014 and 2018 while discharge data in Arles were used since they are available (1990). Rhone River bathymetry was described following the sections and depths of the estuary used by Launay et al. [10] to PK 323. Then, the remaining 7 km come from bathymetric surveys acquired by multibeam in 2012–2013 by the CEREGE.

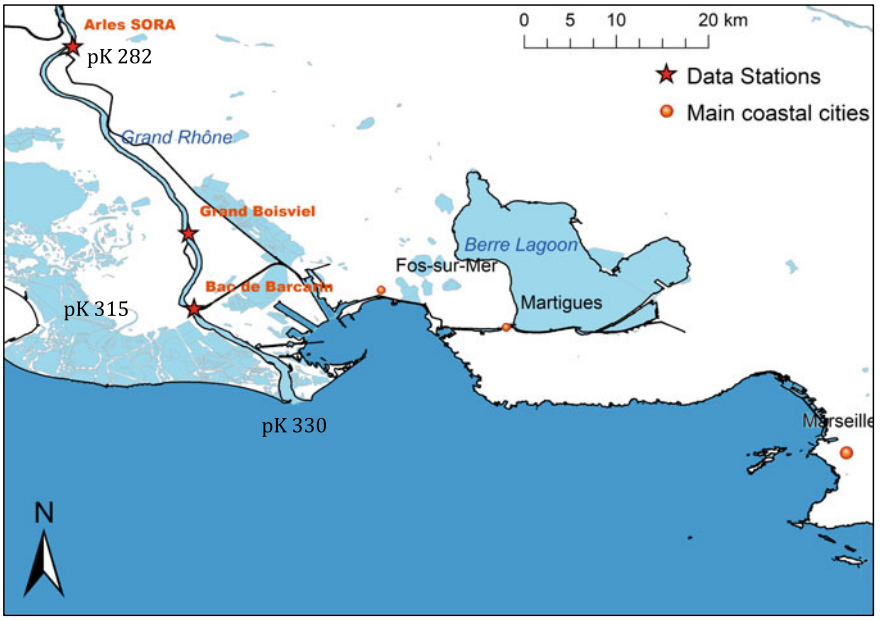

Fig. 71.1 Map of the Gulf of Lion (Mediterranean sea) and Rhone River estuary indicating the locations of discharge, limnimetric and salinity stations used for DRACAR model

71.2.2 An Interface to Describe Estuarine Processes: DRACAR

The implementation of DRACAR in a coupled river-sea continumm model is shown in Fig. 71.2. Box-models are by definition a simplified representation of the system geometry. Theses systems are usually lakes, coastal areas or estuaries [13]. In the

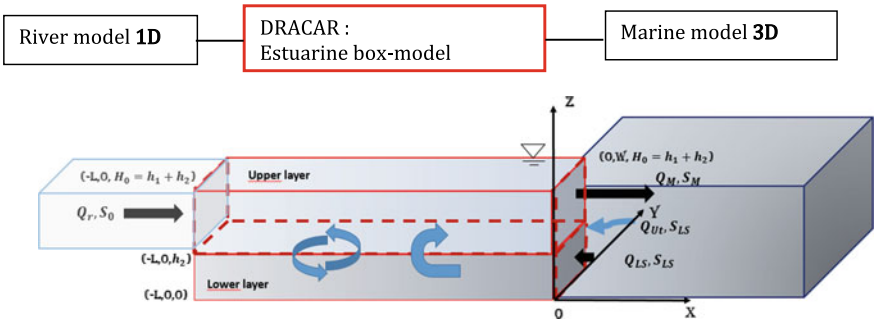

Fig. 71.2 Modelling strategy for the river-sea continuum centered on the "box-model" estuary defined by a length L, width W, mean depth H_0 and layer thicknesses h_1 and h_2 which vary according to hydrological conditions. See text for description of exchanges

case of estuaries, it is strongly recommended to adapt their geometry (box length, interface depth) for a more accurate representation of their dynamics [14].

Here, the box has a length L which is the length of the estuary in terms of freshwater-seawater exchanges. On stratified estuaries this length is the same as the stratification length along the channel. For example, Rhone River salt-wedge length is between 0 and 36 km [11]. The width of the box (W) is the average width of the Rhone estuary, and h_1 and h_2 are the thicknesses of the Rhone plume and the salt-wedge respectively. The dotted lines on Fig. 71.2 represent the interfaces where exchanges of water and salt take place. Flow rates and salinities are represented by arrows at the river and sea boundaries. The physical processes described are the riverine water inflow Q_r at the head of the estuary (here the average discharge in Arles over the last 48 h), the ocean water inflow through the lower layer at the estuary mouth Q_{LS}, the estuarine water outflow through the upper layer at the mouth Q_M with density ρM. The tidal pumping Q_{Ut} over a complete tidal cycle, including the flood and the ebb tide pumping, and resulting in salt intrusion, is represented by the blue horizontal arrow. Turbulent diffusion in all its forms is represented by the coupled blue arrows. Entrainment, which is a "one way process" is represented by a single blue arrow. The color gradient represents the variations in salinity from the river (light shades) to the sea (darker shades).

The methodology is the following. First, define the length of the box and the thickness of the layers with a simple model based on the "coupled shallow water equations" evolving with the river flow conditions. Then, add major estuarine processes such as flow, density and potential energy balance integrated on the box-structure. This leads to a system of 3 equations with 3 unknowns (Q_{LS}, Q_M, ρ_M) that can be solved. Salinity being a conservative tracer, the estuary flushing time F can be calculated, which is a key parameter to describe the geochemistry in an estuary [15].

71.2.3 Stratification Structure Along the Box

Rhone River stratification is reproduced based on the "coupled shallow water equations" applied to salt-wedge estuary from [15] and [16]modified to take into account the river channel slope according to Poggioli and Horner-Devine [17]. They assume that the vertical structure can be represented by two shallow layers of different densities (ρ_0 and ρ_{LS}) and depths (h_1 and h_2) separated by a pycnocline of zero thickness. Also, velocity and density are uniform over each layer, vertical accelerations are negligible, the pressure is hydrostatic, the channel bed slope S_l is soft, and the viscous effects such as friction and turbulence are represented by simple empirical equations which are embedded in the interfacial friction coefficient C_i. Details on the demonstration are available in [18]. They provide in Eq. (71.1) the variation of the non-dimensional depth of the stratification $\varphi = \frac{h_1}{H_O}$ along the non dimensional distance $\chi = \frac{xC_i}{H_0}$ where x is the distance from Rhone River mouth.

$$\frac{d\varphi}{d\chi} = \frac{F_0^2}{\varphi^3 - F_0^2}\left(1 + r\frac{\varphi}{1 - \frac{\chi S_l}{C_i} - \varphi}\right) \tag{71.1}$$

where $r = \frac{\rho_0}{\rho_{LS}}$ is the density ratio and F_0 is the river internal Froude number defined as:

$$F_0 = \frac{\frac{Q_r}{w}}{\sqrt{g(1-r)H_0^3}}, \tag{71.2}$$

In addition, we assumed that Froude number changes over χ due to changes in section and these changes can be approximated by a continuous function (polynomial interpolation in the case of the the Rhone). Equation (71.1) becomes:

$$\frac{d\varphi}{d\chi} = \frac{F(\chi)_0^2}{\varphi^3 - F(\chi)_0^2}\left(1 + r\frac{\varphi}{1 - \frac{\chi S_l}{C_i} - \varphi}\right) \tag{71.3}$$

First boundary condition is that φ at the tip of the salt-wedge equals 1(only fresh-water). The second supposes that the flow is critical at the mouth and that there no other hydraulic control before. In this case, $\varphi = F_0^{2/3}$ [19]. This first order non linear equation is solved with a Runge–Kutta fourth order scheme with R© package "rmutil" [20].

The length of the box L is the value of x at which $h_2 = 0$ (end of stratification and no more salt exchange).

Sea-level variations can be taken into account by adding a variable elevation η_0 (positive or negative) to mean height H_0.

71.2.4 Box-Model Solution

The fundamental governing equations are tidally-averaged (sub-tidal), laterally-averaged, and steady-state. The model consists of four equations: the continuity equation for the volume flux, the salinity equation which includes a parametrization of the tidal pumping, a Potential Energy (PE) equation, and a linear equation of state for seawater. Detailed demonstration is available in [1]. The continuity equation and equations of state are given by:

$$Q_M = Q_{LS} + Q_r \tag{71.4}$$

$$\rho_M Q_M = \rho_{LS} Q_{LS} + \rho_0 Q_r + (\rho_{LS} - \rho_M) a_0 a_t \frac{Q_{Ut}}{2} \tag{71.5}$$

$$\rho = \rho_0(1 + \beta S) \tag{71.6}$$

where $\rho_{M,}$ ρ_{LS} and ρ_0 respectively refers to the densities of the upper and lower layer (generally associated with mean marine water density) at the mouth and river density. The tidal pumping term Q_{Ut} is based on [21, 22] finally β is the haline contraction coefficient.

Q_{Ut} is defined as positive and is the average tidal volume flux during half a tidal cycle.

$$Q_{Ut} = \frac{2}{\pi} U_t W h_1 \tag{71.7}$$

U_t is the tidal current amplitude estimated from the depth-averaged long-wave solution.

$$U_t = \frac{\eta}{H_0}\sqrt{gH_0} \tag{71.8}$$

Using both limnimetric data of Barcarin and Grand boisviel to get the tidal elevation eta we find $U_t = 0.085$ m s^{-1} for the M2 tidal harmonic using the oce package [23]. The geometric coefficient a_t represents the fraction of tidal volume exchange in which the saltier oceanic water replaces estuarine water. a_0 is a calibration coefficient and fixed to 1 as default.

Finally, the potential energy equation is summarized as:

$$PEF_M = PEF_{river} + PEF_{LS} + PEF_{tp} + PEF_{tm} + PEF_{sm} \tag{71.9}$$

The subscripts "tp" and "tm" represent tidal pumping and tidal mixing respectively. The subscript "sm" represents the shear mixing term. Detailed expression of Eq. (71.9) is available in [1]. Formulations for the estuary/box model length L and for the "effective diffusivity" coefficient $K_{v,}$ (results of tidal averaging) are needed in Eq. (71.9). In [1] formulation for L showed limitation on accuracy because it does not take into account the slope of the channel which is a major parameter for salt-wedge intrusion [17]. We rather took the length of the salt-wedge using Eq. (71.3) and finding the length x at which $\varphi = 1$. K_v includes eddy diffusivity and eddy viscosity [24] and is given by:

$$K_v = \left[\frac{\left(A_0 C_D U_t H'\right)^3}{Sc}\right]^{1/3} \tag{71.10}$$

Sc and A_0 are respectively a Schmidt number and a tuning coefficient. In the absence of calibration dataset we took the most used values in the literature which are $Sc = 2.2$ and $A_0 = 0.028$. We define the drag coefficient C_D with Cheezy Manning formula for shallow estuaries:

$$C_D = \frac{gn^2}{\sqrt[3]{H_0}} \tag{71.11}$$

A value of n = 0.27 has been used for Rhone River estuary [25]. H' is a bottom boundary layer height estimate, based on estuary mean salinity horizontal gradient $\frac{d\overline{S}}{dx}$ [26, 24]. This gradient can be found with in-situ data. In this example of strong stratification we consider that the mean horizontal salinity gradient is proportional to the following salt-wedge thickness:

$$\frac{d\overline{S}}{dx} \cong S_{LS}\frac{d\varphi}{dx} \tag{71.12}$$

We found an "effective diffusivity" coefficient K_v of approximately 5×10^{-6} m^2 s^{-1} which is one or two orders of magnitude lower than most observed values in the literature. These small values were not surprising because according to the salt-wedge theory, diffusivity is expected to have minor impact in the mixing compared to entrainment [3].

Finally combination of Eqs. (71.4, 71.5, 71.6, 71.9) with adequate prior salinity structure representation (linear gradient on both layers according to Sun et al. [1]) leads to a polynomial equation $P(Q_{LS})$. Solving the polynomial equation provides Q_{LS}. Then upper layer outflow Q_{UM} and upper layer salinity at the mouth S_{UM} are obtained from Eqs. 71.4 and 71.5.

71.2.5 Estuarine Flushing Time

The flushing time is the time required to replace a solute mass, in an estuary, at the rate of the net flow through the estuary. The flushing time is an important parameter for estuary management dealing with pollutants. It is often used to determine the quantity of a potentially harmful substance an estuary can tolerate before its ecosystem is adversely affected to significant degree. According to Balls [27], flushing time of an estuary partly controls reactivity of trace elements in estuary. For a stratified system, according to Officer [6], the flushing time can be defined as:

$$F = \frac{S_{LS} - S_{UL}}{S_{LS}}\frac{V}{Q_r} \tag{71.13}$$

V is the internal plume volume obtained using estuary width *w*, the depth h_1, and the length of the stratification L obtained in 2.3. S_{UL} is the mean plume salinity calculated as the mean between S_M and S_0 under the hypothesis of linear salinity gradient in the upper layer exposed in the previous section paragraph. This estuarine flushing time can then be compared with the half-reaction time of the geochemical reaction of interest [15] such as cesium desorption from particles.

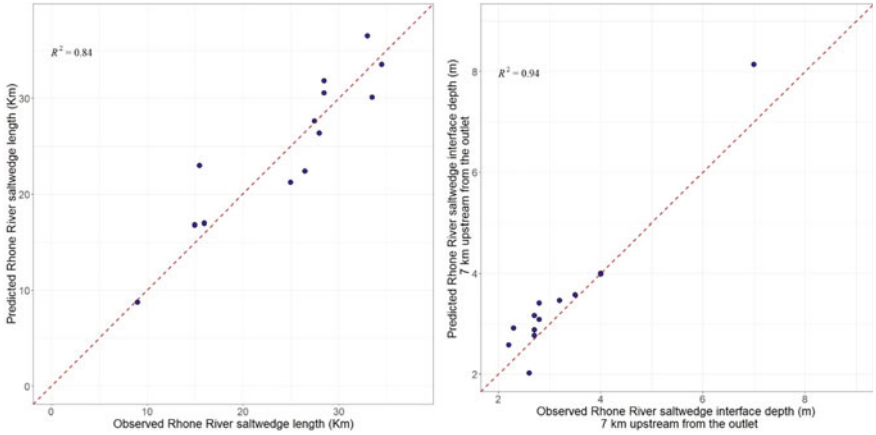

Fig. 71.3 Calibration curves for the length of the salt wedge (left) and the depth of the interface 7 km from the mouth (right) given by the salt-wedge model resulting from the "two layer flow theory" on the Rhone and by the observations at different periods in [11, 28]

71.3 Results

71.3.1 Stratification Structure

The structure of the salt-wedge is calibrated using data from [11, 28] to minimize mean quadratic error on salt-wedge length and interface depth. r was set to the ratio of Rhone River density on Mediterranean sea density. S_l and C_i were allowed to vary for the calibration procedure. Best fit is found for $(S_l; C_i) = (5.0 \times 10^{-5}; 1.7 \times 10^{-4})$. S_l was close to usual slope values for lower-Rhone valley while C_i was in the range of values observed in other mediterranean salt-wedge estuaries [29]. Mean quadratic error for salt-wedge length was 3200 m while mean quadratic error for interface depth was 0.5 m. Observed and modelled structure of the salt-wedge is shown in Fig. 71.3. Results confirm the viability of this approach for estuaries with steady stratification structure over a tidal cycle.

71.3.2 Box-Model Solution

The validity of the model is evaluated by comparing the modelled salinity of the plume (no calibration on A_0, a_0 and Sc) with the observed plume salinity at "Barcarin" (15 km upstream from the mouth). Using the hypothesis of salinity linear increase from S_0 at the tip of the salt-wedge to S_{UM} at the river mouth, the salinity at this location is:

$$\begin{cases} S_{(X=15{,}000)} = S_0 \frac{15{,}000}{L} + S_M\left(1 - \frac{15{,}000}{L}\right) & L \geq 15{,}000 \\ S_{(X=15{,}000)} = S_0 & L < 15{,}000 \end{cases} \quad (71.14)$$

The comparison of the predicted salinity chronicles at Barcarin with the average salinity of the last 48 h at Barcarin is presented on Fig. 71.4 over 8.5 months in 2017–2018. We observe that all the salinity peaks are well reproduced as well as the periods of absence of the salt wedge (salinity of 0.2). However the model sometimes presents a delay when compared with the observations. This result is not surprising since the model is in a steady state and thus, poorly assumes transient effects.

Box-model performances for salinity prediction of Fig. 71.4 are reported in Table 71.1, and are compared with those using a power-law regression ($S_{(X=15{,}000)}$=7.012

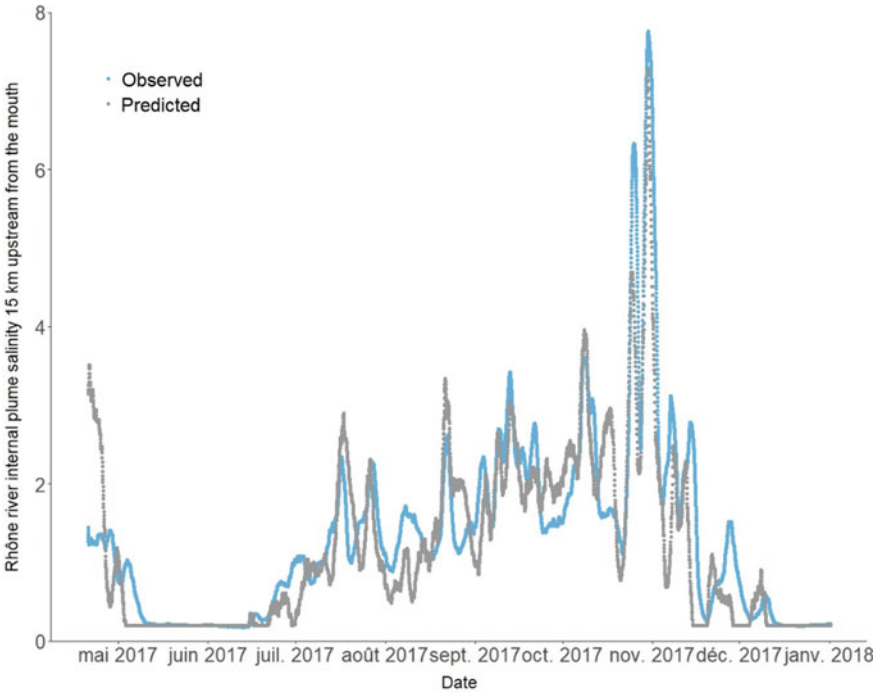

Fig. 71.4 Comparison of the salinity chronicles predicted at Barcarin (PK 315) and the average salinity observed over the last 48 h at Barcarin

Table 71.1 Comparison of the salinity modeling performance at Barcarin between the box-model and a power regression as a function of the flow

Number of data	Coefficient	R_2	RMSE	NSE	BIAS	Skill (Index of agreement)
N = 28,237	DRACAR	0.73	0.50	0.72	−0.06	0.92
N = 28,237	S = f(Q_r)	0.76	0.47	0.76	−0.04	0.93

$\times 10^6 Q_r^{-2.358}$). Equations of "goodness of fit" coefficients are given in [30]. Results are slightly better when using the regression but DRACAR does not rely on salinity data while the regression curve is empirical and based on these observations. These good performances are partly due to the prior estimation of box-length with the coupled shallow water equations (derived from Eq. 71.3). Precised river inputs to the sea in terms of flows and salinity can be implemented in the coastal hydrodynamic model following [1, 31].

71.3.3 Discussion on Rhone River Plume Reactivity Toward Radiocesium

Cesium radioactive isotopes (^{134}Cs and ^{137}Cs) have been extensively monitored in the environment due to their significant radioecological hazard and their persistence (half-life of 2.4 and 30.2 years respectively). They are produced through uranium fission within nuclear reactors and thus can be found in case of accident or authorized releases. Cesium exists in rivers as dissolved Cs with small tendency to form colloids but is mainly transported in particular form because of its high affinity for clay minerals. At the river-sea interface, the important changes in physico-chemical conditions including ionic strength, solution composition and pH may induce the desorption of Cs from particles to the dissolved phase. This fluxe to the dissolved phase can be significant and is a major source of uncertainties. However this reaction has not been observed in all estuaries.

According to a review of laboratory experiments, radiocesium release in dissolved phase follows two parallel first-order kinetics [4]. The main involved kinetic is the faster one with a half-reaction time of one hour. In addition, this study suggests that low salinity is likely to trigger these reactions (potential salinity threshold of 3). This hypothesis is supported by recent lab experiments carried out on Rhône River (unpublished).

To assess the Rhone estuary capability to trigger salinity threshold, different case study of Rhone River discharge were investigated. The mean Rhone River discharge over 48 h was set to 1500, 950 and 520 m^3/s for cases a, b and c respectively. The mean Rhone River discharge observed in Arles is 1500 m^3/s while discharges under 950 m^3/s are observed less than 30% of the time [25]. Sea level variation was not taken into account. DRACAR was run for each of these cases to describe seawater intrusion, mean Rhone River plume salinity (from the tip of the walt-wedge to Rhone River mouth) and flushing time. Outputs of the modelling are summarized in Table 71.2. Mean quadratic errors on salt-wedge length and interface depth obtained in 3.1 are propagated in the flushing time calculation.

In case (a), the salt-wedge was blocked at the mouth and no significant intrusion (less than 1 km) was modelled. For lower discharges, significant intrusion of 12 km (case b) and 32 km (case c) lengths occurred. Stratification structure from the Rhone River mouth to the Seuil de Terrin is shown in Fig. 71.5 for the significant intrusion

Table 71.2 Summary of simulations results of DRACAR for 3 different Rhone River discharge scenario

Case	River discharge (m^3/s)	Salt-wedge length (km)	Estuarine discharge Q_{UM} (m^3/s)	Salinity at estuary mouth S_{UM}	Mean salinity upper layer S_{UL}	Flushing time (hours)
a	1500	0	0			
b	950	12	970	2	1.1	9 ± 3.8 h
c	520	32	610	5.8	3	25.5 ± 6.5 h

cases (b) and (c).

According to Table 71.2, Rhone water is brackish on its last kilometers before the outlet at discharges inferior to mean discharge. Salt-wedge induces a landward flow of 20 m^3/s (case b) to 90 m^3/s (case c).These results are similar with those of [29] who found a landward flow ranging between 3 and 15% of the river flow. When the discharge is of 950 m^3/s, the Rhone River is not brackish enough to trigger salinity desorption (threshold of 3) even at the mouth ($S_{UM} = 2$). For discharges of 520 m^3/s and lower, the mean Rhone River plume salinity is equal or superior to the salinity threshold. Flushing times of Rhone River estuary are small compared to others estuary [32]. Yet, they are high enough for a significant cesium desorption process given its half reaction time of one hour. This process increases dissolved radiocesium fluxes to the sea.

71.4 Conclusion

Rhone River discharge lower than 1500 m^3/s allows a salt wedge intrusion. The associated landward flow starts to propagate upstream and progressively modifies the Rhone River circulation in its estuarine domain. Landward flow and salinity at the river mouth provided by the box-model can be implemented into a coastal ocean model to increase the realism of riverine inputs to the sea.

With a discharge of 520 m^3/s or lower, the salt-wedge reaches the "Seuil de Thibert" and the Rhone River plume meets the conditions to trigger cesium desorption from particles (mean salinity superior to 3 and flushing time far superior to half reaction time) and to increase dissolved fluxes to the sea. This critical low-flow scenario has a weak frequency of occurrence but happens during few days every summer. Finally, the source term accounting for estuarine processes can be implemented into marine radionuclide dispersion models used in case of accidental releases [33].

In our study, the model calibration was restricted to the structure of the box-model. Results confirm the importance of taking into account estuary dimensions (length, depth of the stratification) variability according to hydrodynamic conditions [14]. Taking into account the slope for highly stratified estuaries also seems to be an interesting improvement. Better consideration of the geometry, in particular the exchange

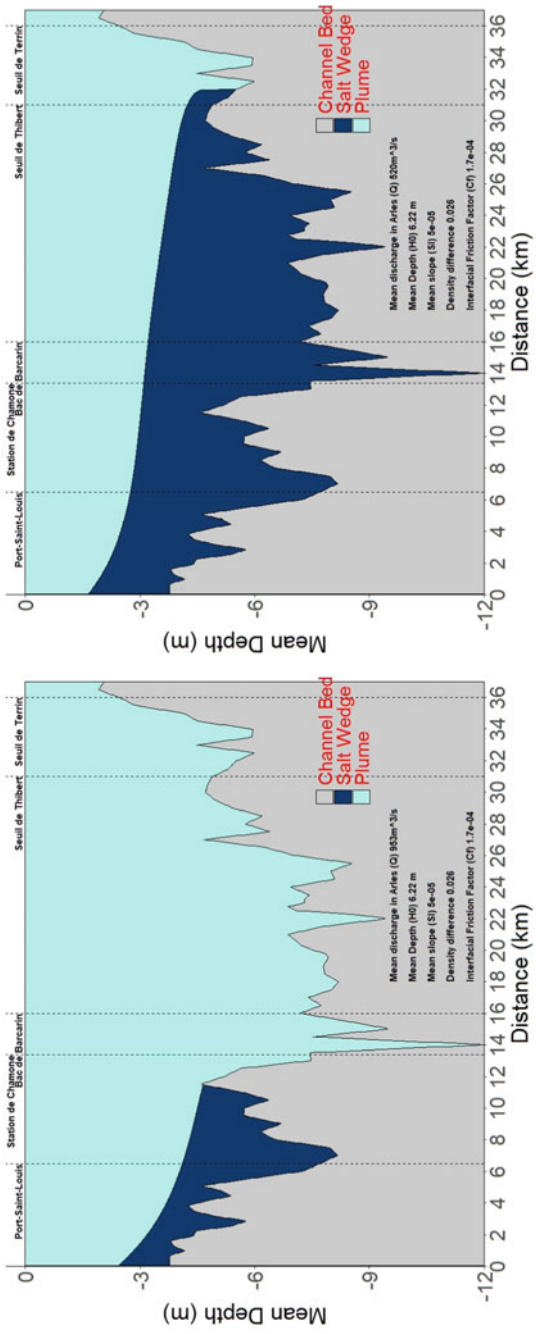

Fig. 71.5 Longitudinal description of the Rhone River salt-wedge (dark blue) for two different conditions (river discharge of 520 m^3/s on the left and 950 m^3/s on the right). The Rhone River plume is in light-blue. The x-axis is the distance from the Rhone River mouth

surfaces, constrains the calibration coefficients (here A_0 and a_0) and ultimately makes it possible to differentiate and specify physical processes.

The sufficient performance of this box-model on the Rhone River estuary confirms its usefulness on salt wedge estuaries. Hydrodynamics and solutes dynamics are also adaptable to other estuarine systems with higher tidal ranges and convergent channel [1, 17] by using a more accurate definition of the tidal pumping term. However, choices have to be made on assumptions and simplifications for suspended sediments dynamics. Other pollutants reactivity in this interface zone can be treated with this approach.

References

1. Sun Q, Whitney MM, Bryan FO, Heng Tseng Y (2017) A box model for representing estuarine physical processes in Earth system models. Ocean Model 112:139–153. https://doi.org/10.1016/j.ocemod.2017.03.004
2. Eyrolle F et al (2020) Radionuclides in waters and suspended sediments in the Rhone River (France)—current contents, anthropic pressures and trajectories. Sci Total Environ, p 137873. https://doi.org/10.1016/j.scitotenv.2020.137873
3. Dyer KR (1997) Estuaries a physical introduction, 2nd edn.
4. Delaval A, Duffa C, Radakovitch O (2020) A review on cesium desorption at the freshwater-seawater interface. J Environ Radioact 218:106255. https://doi.org/10.1016/j.jenvrad.2020.106255
5. Zhou N, Westrich B, Jiang S, Wang Y (2011) A coupling simulation based on a hydrodynamics and water quality model of the Pearl River Delta, China. J Hydrol 396(3–4):267–276. https://doi.org/10.1016/j.jhydrol.2010.11.019
6. Officer CB (1980) Box models revisited. Mar Sci 11:65–114. https://doi.org/10.1007/978-1-4757-5177-2_4
7. Shiller AM (1996) The effect of recycling traps and upwelling on estuarine chemical flux estimates. Geochim Cosmochim Acta 60(17):3177–3185. https://doi.org/10.1016/0016-7037(96)00159-7
8. Boudet L, Sabatier F, Radakovitch O (2017) Modelling of sediment transport pattern in the mouth of the Rhone delta: role of storm and flood events. Estuar Coast Shelf Sci 198:568–582. https://doi.org/10.1016/j.ecss.2016.10.004
9. Eyrolle F et al (2012) Consequences of hydrological events on the delivery of suspended sediment and associated radionuclides from the Rhône River to the Mediterranean Sea. J Soils Sediments 12(9):1479–1495. https://doi.org/10.1007/s11368-012-0575-0
10. Launay M, Dugué V, Faure JB, Coquery M, Camenen B, Le Coz J (2019) Numerical modelling of the suspended particulate matter dynamics in a regulated river network. Sci Total Environ 665:591–605. https://doi.org/10.1016/j.scitotenv.2019.02.015
11. Ibañez C, Pont D, Prat N (1997) Characterization of the Ebre and Rhone estuaries: a basis for defining and classifying salt-wedge estuaries. Limnol Oceanogr 42(1):89–101. https://doi.org/10.4319/lo.1997.42.1.0089
12. Sakho I et al (2019) Suspended sediment flux at the Rhone River mouth (France) based on ADCP measurements during flood events. Environ Monit Assess 191(8). https://doi.org/10.1007/s10661-019-7605-y
13. Larsen J, Mohn C, Timmermann K (2013) A novel model approach to bridge the gap between box models and classic 3D models in estuarine systems. Ecol Modell 266(1):19–29. https://doi.org/10.1016/j.ecolmodel.2013.06.030
14. MacCready P, Geyer WR (2009) Advances in estuarine physics. Ann Rev Mar Sci 2(1):35–58. https://doi.org/10.1146/annurev-marine-120308-081015

15. Morris AW (1990) Kinetic and equilibrium approaches to estuarine chemistry. Sci Total Environ 97–98(C):253–266. https://doi.org/10.1016/0048-9697(90)90244-O
16. Schijf JB, Schonfeld JC (1953) Theoretical considerations on the motion of salt and fresh water. In: Proceedings of Minnesota international hydraulics convention, pp 321–333
17. Poggioli AR, Horner-Devine AR (2015) The sensitivity of salt wedge estuaries to channel geometry. J Phys Oceanogr 45(12):3169–3183. https://doi.org/10.1175/JPO-D-14-0218.1
18. Krvavica N, Ružić I (2019) Assessment of sea-level rise impacts on salt-wedge intrusion in idealized and Neretva River Estuary. Estuar Coast Shelf Sci 234(December):2020. https://doi.org/10.1016/j.ecss.2020.106638
19. Geyer WR, Ralston DK (2012) The dynamics of strongly stratified estuaries, vol 2. Elsevier Inc.
20. Swihart B, Lindsey J (2020) Package ' rmutil,'
21. Stommel H, Farmer HG (1952) On the nature of Estuarine circulation
22. MacCready P (2004) Toward a unified theory of tidally-averaged estuarine salinity structure. Estuaries 27(4):561–570. https://doi.org/10.1007/BF02907644
23. Kelley D, Clarks R, Layton C (2020) Package 'oce
24. MacCready P, Geyer WR (2010) Advances in Estuarine physics. Ann Rev Mar Sci 2(1):35–58. https://doi.org/10.1146/annurev-marine-120308-081015
25. Boudet L (2017) Modélisation du transport sédimentaire lié aux crues et aux tempêtes à l'embouchure du Rhône. Aix-Marseille
26. Monismith SG, Burau J, Stacey M (1996) Stratification dynamics and gravitational circulation in Northern San Francisco Bay. In: Hollibaugh JT (ed) EdSan Francisco Bay Ecosystem. American Association for the Advancement of Science, pp 123–153
27. Balls PW (1994) Nutrient inputs to Estuaries from Nine Scottish East coast rivers; influence of Estuarine processes on inputs to the North Sea. Estuar Coast Shelf Sci 39(4):329–352. https://doi.org/10.1006/ecss.1994.1068
28. Levasseur L, Doutriaux E (1992) 5. Le coin salé du Grand Rhône et les travaux de creusement du seuil de Terrin, pp 15–17
29. Krvavica N, Travaš V, Ožanić N (2016) A field study of interfacial friction and entrainment in a microtidal salt-wedge estuary. Environ Fluid Mech 16(6):1223–1246. https://doi.org/10.1007/s10652-016-9480-1
30. Zambrano-Bigiarini M (2020) Package ' hydroGOF
31. Verri G, Pinardi N, Bryan F, Heng Tseng Y, Coppini G, Clementi E (2020) A box model to represent estuarine dynamics in mesoscale resolution ocean models. Ocean Model 148. https://doi.org/10.1016/j.ocemod.2020.101587
32. Dürr HH, Laruelle GG, van Kempen CM, Slomp CP, Meybeck M, Middelkoop H (2011) Worldwide typology of nearshore coastal systems: defining the Estuarine filter of river inputs to the oceans. Estuaries Coasts 34(3):441–458. https://doi.org/10.1007/s12237-011-9381-y
33. Duffa C, Bailly P, Caillaud M, Charmasson S, Renaud P (2016) Development of emergency response tools for accidental radiological contamination of French coastal areas. J Environ Radioactivity 151:487–494. https://doi.org/10.1016/j.jenvrad.2015.04.019